Acquisition Time in Laser Inter-Satellite Link Under Satellite Vibrations

Kwanyong Lee, Vuong Mai, *Member, IEEE*, and Hoon Kim, *Senior Member, IEEE*

***Abstract*—Pointing, acquisition, and tracking (PAT) is a major technical challenge of laser inter-satellite links (ISLs). For the fast establishment of laser link and the maximization of communication time, it is of importance to minimize the acquisition time. Satellite vibrations affect the PAT procedure adversely, and thus serve to increase the acquisition time. In this paper, we investigate through theoretical analysis the average acquisition time of laser ISLs in the presence of satellite vibrations. The analytic expression about the time taken from the beginning of spiral scan to the acquisition of the scan beam is provided in the presence of the pointing errors caused by vibrations. We also derive the optimum beam divergence angle for the acquisition time. The analyses are validated by Monte-Carlo computer simulations and a proof-of-concept experiment. The results show that the acquisition time can be minimized by adjusting the beam divergence angle adaptively to the link conditions.**

***Index Terms*—Free space optical communications, inter-satellite links, PAT, spatial acquisition.**

I. Introduction

LASER intersatellite links (ISLs), thanks to the use of unlicensed optical spectrum, enormous transmission capacity, and narrow beam divergence, are gaining popularity as a future-proof technology potentially replacing the traditional radio-frequency links [1], [2], [3], [4]. In laser ISLs, the major technical challenge is the pointing, acquisition, and tracking (PAT) [5], [6], [7]. Long transmission distance (e.g., >1000 km) together with the use of narrow-divergence optical beam (e.g., tens of μrad) makes the PAT a daunting task especially when the relative velocity of the satellites is high. Vibrations of satellite caused by thruster firing and the mechanical moving components such as reaction wheels make the PAT even more challenging [8].

The PAT procedure in laser ISLs starts with the location estimation of the transmitter and receiver satellites. With the aid of global positioning system (GPS) and two-line element (TLE) data sets, the location of the satellite can be identified. The locations of the counter satellites can also be identified by the orbital determination, which is estimated from the TLE data processed by the simplified perturbation models [9]. After the satellites identify the locations of counter satellite, the transmitter satellite rotates its body and/or steers the optical transmitter toward where the receiver satellite is expected to be located. The direction of the receiver aperture is also steered to the direction of the transmitter satellite. After this pointing procedure, the satellites attempt to pinpoint the location of the counter satellites. For this purpose, the transmitter satellite scans the uncertainty cone using a wide-divergence optical beam (or beacon). The size of the uncertainty cone is mainly determined by the accuracy of the orbital determination and the attitude error of the transmitter satellite [6]. The spiral scan is commonly utilized for the acquisition. Starting from the location where the counter satellite is expected to be located, the optical beam spirals outward to cover the uncertainty cone. Whenever the receiver satellite detects the scan beam, it sends the optical beam acknowledging the reception of the scan beam back to the transmitter satellite [10]. The array detector having a wide field of view (such as a focal plane array) is typically employed for the direction detection of the optical beam. Finally, the transmitter satellite also acquires the location of the receiver satellite by detecting this feedback optical beam sent from the receiver satellite.

To facilitate the acquisition, a beacon light composed of a wide-divergence optical beam can be employed [11], [12], [13], [14]. In this beacon-based system, the wide-divergence beam should be handed off to a narrow-divergence one for communications after the acquisition procedure. On the other hand, a beaconless system utilizes a narrow-divergence communication beam for both acquisition and communication [15], [16], [17]. Since the beaconless system does not require an extra beacon transmitter, it reduces the implementation complexity at the expense of a long acquisition time.

In laser ISLs, it is highly desirable to minimize the acquisition time, which is defined by the time that it takes from the beginning of the scan to the acquisition of the scan beam at the counter satellite. This is because laser ISLs might have narrow communication time windows due to the high velocity of satellites. A long acquisition time would make these windows even narrower. Also, the laser ISLs could be disrupted unexpectedly, for example, by misalignment, solar conjunction, blocking of a line-of-sight path, etc. In this case, the satellites attempt to re-establish the link through the PAT procedure. For rapid re-establishment of the link, it is also necessary to minimize the acquisition time.

There have been a few efforts to reduce the acquisition time. For example, the optimum size of uncertainty cone was studied

Manuscript received 9 May 2023; revised 27 June 2023; accepted 30 June 2023. Date of publication 3 July 2023; date of current version 12 July 2023. This work was supported by the grant-in-aid of Hanwha Systems. *(Corresponding author: Hoon Kim.)*

Kwanyong Lee and Hoon Kim are with the School of Electrical Engineering, Korea Advanced Institute of Science and Technology, Daejeon 34141, South Korea (e-mail: haldamir3@kaist.ac.kr; hoonkim@kaist.ac.kr).

Vuong Mai is with the Faculty of Engineering and Informatics, University of Bradford, BD7 1DP Bradford, U.K. (e-mail: m.v.vuong@ieee.org).

Digital Object Identifier 10.1109/JPHOT.2023.3291807

in [18] to reduce the acquisition time. Instead of using the commonly used 3σ, where σ represents the angular standard deviation of the location uncertainty of counter satellite, the authors reduced the size of uncertainty cone to 1.3σ even though it could increase the repetition of the scan. In another study, the acquisition time was reduced by suppressing the attitude determination error with the aid of a star sensor [19]. However, the orbital determination errors, which mainly affect the size of uncertainty cone in low-earth orbit (LEO)-to-LEO satellite links, were not considered in this study. The optimum beam divergence angle of scan beam for acquisition time was derived in [10]. For an elliptically shaped optical beam, this work analyzed the optimum beam divergence angle for the acquisition time theoretically when the raster scan was employed for short-range communications. However, none of these works takes into account the impact of vibrations on the acquisition time.

It is inevitable that satellites experience mechanical vibrations caused, for example, by thruster firing and mechanical moving components. It was shown that the angular fluctuations caused by these mechanical vibrations can be as high as a few tens of microradians [8]. Mechanical vibrations of the satellite serve to distort the spiral trajectory of the scan beam during the acquisition procedure, and thus make the scan beam fail to cover the entire region of the uncertainty cone. Since the hit probability, defined by the average probability of acquiring the scan beam successfully, of a single scan decreases in the presence of vibrations, multiple scans are required to increase the overall hit probability [16]. As a result, the acquisition time should be increased. A couple of previous works presented the impact of vibrations on the hit probability and acquisition time. However, the authors in [16] relied solely on simulation for estimating the acquisition time. The work presented in [20] showed the theoretical analysis on the hit probability for some cases. Even though this work provided theoretical insight about the hit probability, it is not easy to apply this theory to estimate the overall hit probability. To the best of our knowledge, there has been no theoretical study on the overall hit probability and acquisition time applicable to the entire scan region for various amounts of vibration.

In this paper, we present the theoretical analysis of the acquisition time in the presence of satellite vibrations. Also, we provide the optimized beam divergence angles for acquisition time. The beam divergence angle can be adjusted adaptively to the link conditions to minimize the acquisition time in laser ISLs. To validate our theoretical analysis, we perform Monte-Carlo computer simulations and a proof-of-concept experiment. We show that the acquisition time can be reduced considerably over a wide range of transmission distances by utilizing the adaptive beam control technique.

The rest of this paper is organized as follows. In Section II, we present the theoretical analysis of acquisition time, optimum beam divergences, and hit probability. We compare the theoretical analysis with Monte-Carlo simulations and also demonstrate the effectiveness of the adaptive beam control technique in reducing the acquisition time in Section III. We carry out the proof-of-concept experiment and present the results in Section IV. Finally, Section V concludes the paper.

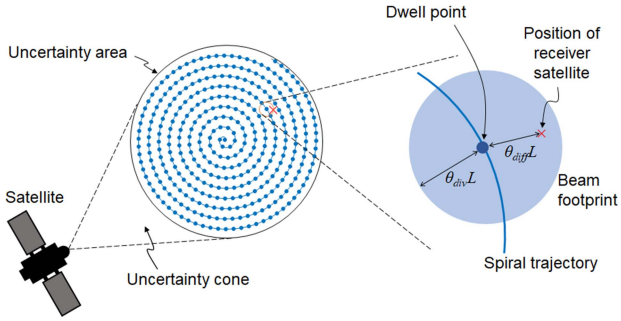

Fig. 1. Spiral trajectory of scan beam.

II. Theoretical Analysis

The transmitter satellite scans the uncertainty cone to search for the accurate location of the counter satellite using a scan beam. Fig. 1 shows the spiral trajectory of the scan beam on the receiver's aperture plane. The scan beam can be either a beacon or a communication beam (for the beaconless system). Starting from the center of the uncertainty area, the scan beam spirals outward to cover the entire region of the uncertainty area. The scan beam stays at certain positions called dwell points on the spiral trajectory for the dwell time before it moves to another dwell point. If the receiver satellite detects the beacon signal, the feedback signal is transmitted to the transmitter satellite and the acquisition procedure ends by the transmitter satellite detecting this feedback signal (sent from the receiver satellite).

In this work, we assume that the scan beam has a Gaussian intensity profile having a half angle of beam divergence θ_{div}, where the intensity drops to $1/e^2$ of the maximum value. The intensity of the scan beam can be expressed as [21]

$$I_{beam} = \frac{2P_t}{\pi L^2 \theta_{div}^2} \exp\left(-\frac{2r_z^2}{L^2\theta_{div}^2}\right) \tag{1}$$

where P_t is the transmitted optical power and r_z is the radial distance from the center of the beam. If the beam footprint (on the aperture plane) is much larger than the aperture size, the optical power impinging onto the aperture of the receiver satellite can be expressed approximately as [22]

$$P_{rec} = \frac{2P_t A_{rec}}{\pi L^2 \theta_{div}^2} \exp\left(-\frac{2\theta_{diff}^2}{\theta_{div}^2}\right) \tag{2}$$

where θ_{diff} is the angular deviation of the receiver satellite from the nearest dwell point and L is the transmission distance. Also, A_{rec} is the area of the receiver aperture, which is expressed by πr_{rec}^2, where r_{rec} is the radius of the receiver aperture. For the dwell time of T_{dw}, the receiver satellite can detect the scan beam when the following relation is satisfied.

$$E_{th} \leq P_{rec} T_{dw} \tag{3}$$

Here, E_{th} is the threshold energy required to detect the scan beam. It might include some margin on top of the minimum required energy to guarantee the detection. We define the effective angle of scan beam as the maximum θ_{diff} satisfying the

inequality of (3). Then, it can be expressed as

$$\theta_{eff} = \sqrt{\frac{1}{2}\theta_{div}^2 \ln\left(\frac{2T_{dw}P_tA_{rec}}{\pi L^2\theta_{div}^2 E_{th}}\right)} \tag{4}$$

We design the spiral trajectory of spatial acquisition by using the effective angle of scan beam. The spiral trajectory represented by its radius (r) and angle (θ) in the polar coordinates with the origin at the center of the uncertainty area can be expressed as

$$r = v_r\, t \tag{5}$$

$$\theta = v_\theta\, t \tag{6}$$

where t is time. Here, the radial and angular velocities are expressed by using the effective angle of scan beam as

$$v_r = \sqrt{\frac{2\,(1-k)\,\theta_{uc}\theta_{eff}^2}{\pi t\,(\theta_{uc}-\theta_{eff})\,T_{dw}}} \tag{7}$$

$$v_\theta = \sqrt{\frac{2\pi\,(\theta_{uc}-\theta_{eff})}{(1-k)\,\theta_{uc}tT_{dw}}} \tag{8}$$

where k is the overlap factor and θ_{uc} is the half angle of the uncertainty cone [17].

The scan time taken from the initial point (00) in the uncertainty area to a point (r_p,θ_p) is expressed approximately as [17], [18]

$$T_a\,(r_p) \approx \frac{\pi T_{dw}}{2\,(1-k)}\left(\frac{r_p}{\theta_{eff}}\right)^2 \tag{9}$$

The scan time to cover the entire uncertainty cone is then written as

$$T_{scan} \approx \frac{\pi T_{dw}}{2\,(1-k)}\left(\frac{\theta_{uc}}{\theta_{eff}}\right)^2 \tag{10}$$

When the receiver satellite detects the scan beam, the acquisition procedure ends. We assume that the location error of the receiver satellite follows the 2-dimensional Gaussian distribution with zero means. The probability density function (PDF) of angular error is then given by [18]

$$f_G\ (\theta_{v,h}) = \frac{1}{\sqrt{2\pi}\sigma_{v,h}}\ \exp\left(-\frac{\theta_{v,h}^2}{2\sigma_{v,h}^2}\right) \tag{11}$$

where $\theta_{v,h}$ is vertical and horizontal error angle and $\sigma_{v,h}$ is the standard deviation of the vertical and horizontal error angle. We assume the vertical and horizontal errors have the same standard deviations. Then, the radial location error can be expressed as the Rayleigh distribution of a scale factor of σ_r (where $\sigma_r = \sigma_v = \sigma_h$). Thus, the PDF of the angle from the transmitter subtended by the line connecting the center of the uncertainty area and the location of the receiver satellite is given by

$$f_R\,(\theta_R) = \frac{1}{\sqrt{2\pi\sigma_r^2}}\ \exp\left(-\frac{\theta_R^2}{2\sigma_r^2}\right) \tag{12}$$

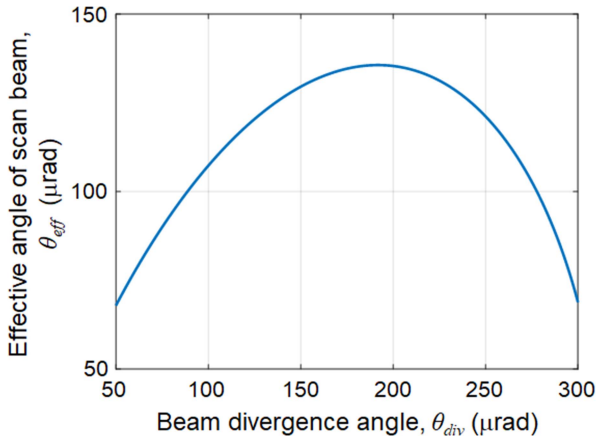

Fig. 2. Effective angle of scan beam as a function of the beam divergence angle.

where σ_r is the scale parameter. The average acquisition time for the single scan is given by

$$T_{avg} = \int_0^{\theta_{uc}} T_a\,(\theta)\, f_R\,(\theta)\, d\theta \tag{13}$$

Substituting T_a of (9) and f_R of (12) into (13), we have

$$T_{avg} = \frac{\pi T_{dw}\sigma_r^2}{(1-k)\,\theta_{eff}^2}\left[1-\left(\frac{\theta_{uc}^2}{2\sigma_r^2}+1\right)\exp\left(-\frac{\theta_{uc}^2}{2\sigma_r^2}\right)\right] \tag{14}$$

It shows that the average acquisition time for single scan is inversely proportional to the square of the effective angle of scan beam. Thus, we can minimize the average acquisition time by maximizing θ_{eff}.

Fig. 2 shows the effective angle of scan beam expressed by (4) as a function of the divergence angle of the scan beam. In this plot, the transmission distance, dwell time, and transmitter optical power are set to be 1000 km, 2 ms, and 1 W, respectively. Also, we set the radius of receiver aperture to be 5 cm and the threshold energy for the detection of scan beam to be 100 pJ [16]. The figure clearly shows that there exists a maximum effective angle of scan beam. This is because the optical power density per unit area decreases as the beam divergence increases. The maximum effective angle of scan beam can be obtained from (4) as

$$\theta_{eff,opt} = \frac{0.6065}{L}\sqrt{\frac{T_{dw}P_tA_{rec}}{\pi E_{th}}} \tag{15}$$

The divergence angle which gives us the maximum effective angle of scan beam is given by

$$\theta_{div,opt} = \frac{0.8578}{L}\sqrt{\frac{T_{dw}P_tA_{rec}}{\pi E_{th}}} \tag{16}$$

We can see the optimum divergence angle of scan beam for the acquisition time depends on the parameters such as the transmission distance, dwell time, and receiver aperture. This implies that it is necessary for the transmitter satellite to obtain those parameters before the acquisition procedure. It is interesting to note that only L is a variable and other parameter are fixed.

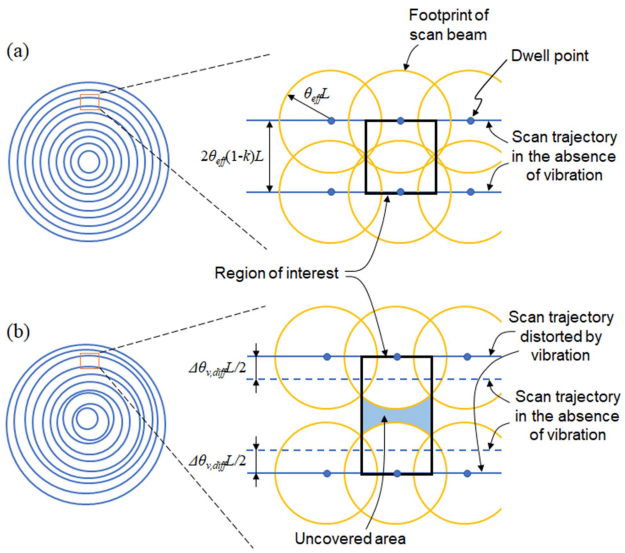

Fig. 3. Spiral trajectory modeled as multiple rings (a) in the absence of vibration and (b) in the presence of vibration.

The link distance can be readily estimated from the TLE data processed by the simplified perturbation models. On the other hand, a couple of parameters pertinent to the receiver satellite could be given as fixed parameters or could be exchanged between the satellites through an RF auxiliary channel [23].

One way to realize the optimum divergence angle of scan beam for the acquisition time is to employ the adaptive beam control (ABC) [23], [24], [25]. In this technique, the beam divergence angle is adjusted adaptively to the link conditions by using a variable focus liquid lens. It was also experimentally demonstrated that both the beam steering and ABC can be realized by using an on-axis variable focus lens (VFL) followed by two decentered VFLs [26].

The spiral trajectory should be designed to cover the uncertainty area. However, the satellite vibrations distort the scan trajectory and make the scan beam fail to cover the entire region of the uncertainty area. This reduces the hit probability of a single scan, and consequently increases the acquisition time since multiple scans should be conducted [16].

We estimate the acquisition time theoretically in the presence of satellite vibrations. Fig. 3 shows a part of spiral trajectory covered by scan beam's footprints (on the receiver's aperture plane). The spiral trajectory can be modeled as multiple co-centered rings separated by $2\theta_{eff}(1-k)L$, as shown in Fig. 3(a). This figure also shows a part of two adjacent rings. The arcs of rings are illustrated as straight lines in the figure. We assume that adjacent footprints of the scan beam on a ring experience the same amount of vibrations. This is because the dwell time is much shorter than the time scale of satellite vibrations. For example, we can set the dwell time to be a few milliseconds, whereas the mechanical vibrations have frequency components mainly below 100 Hz [8]. However, angular fluctuations caused by mechanical vibrations could affect the center position of the rings, as shown in Fig. 3(b). Thus, we assume that the mechanical vibrations affect the distances between rings in the spiral trajectory without changing the distance between the adjacent footprints of scan beam. Fig. 3(b) shows a part of scan trajectory distorted by vibrations, also modeled as rings. In this figure, the scan trajectory is shifted by $\Delta\theta_{v,diff}L/2$ from its undistorted one. The distorted trajectory creates a region uncovered by the footprints of scan beam. We can estimate the hit probability from the ratio of the uncovered area, A_{unc}, to the area of region of interest, $2L^2\theta_{eff}^2(1-k)$. We then calculate the uncovered area as follows:

a) If $0 \le \Delta\theta_{v,diff} \le (\sqrt{3}-2+2k)\theta_{eff}$,

$$A_{unc}\ (\Delta\theta_{v,diff}) = 0 \tag{17}$$

b) If $(\sqrt{3}-2+2k) < \Delta\theta_{v,diff} \le 2k\theta_{eff}$,

$$A_{unc}\ (\Delta\theta_{v,diff}) = 4L^2 \int_{\frac{\sqrt{3}}{2}\theta_{eff}}^{\theta_{eff}(1-k)+\Delta\theta_{v,diff}/2} \left(\frac{\theta_{eff}}{2} - \sqrt{\theta_{eff}^2 - \theta'^2}\right) d\theta' \tag{18}$$

c) If $2k\theta_{eff} < \Delta\theta_{v,diff} \le \sqrt{3}\theta_{eff}$,

$$A_{unc}\ (\Delta\theta_{v,diff}) = 2L^2\theta_{eff}\ (\Delta\theta_{v,diff}/2 - k\theta_{eff}) + 4L^2 \int_{\frac{\sqrt{3}}{2}\theta_{eff}}^{\theta_{eff}} \left(\frac{\theta_{eff}}{2} - \sqrt{\theta_{eff}^2 - \theta'^2}\right) d\theta' \tag{19}$$

d) If $\sqrt{3}\theta_{eff} \le \Delta\theta_{v,\,diff} < 2\theta_{eff}$,

$$A_{unc}\ (\Delta\theta_{v,diff}) = 2L^2\theta_{eff}\ (\Delta\theta_{v,diff}/2 - k\theta_{eff}) + 4L^2 \int_{\Delta\theta_{v,diff}/2}^{\theta_{eff}} \left(\frac{\theta_{eff}}{2} - \sqrt{\theta_{eff}^2 - \theta'^2}\right) d\theta' \tag{20}$$

e) If $2\theta_{eff} \le \Delta\theta_{v,diff}$,

$$A_{unc}\,(\Delta\theta_{v,diff}) = 2L^2\theta_{eff}^2\ (1-k) \tag{21}$$

It is worth noting that when an instantaneous vibration is large the uncovered area shown in Fig. 3(b) could be covered by the beam footprints on the other rings (not illustrated in this figure). This happens when the instantaneous vibration is larger than the distance between rings, i.e., $\Delta\theta_{v,diff}L/2 > 2\theta_{eff}(1-k)L$. To take this into account, we calculate the area covered by the scan beam from the other rings for given θ_{vib} and $\Delta\theta_{v,diff}$, which is denoted by A_{cov}. We assume that the satellite vibrations follow the Gaussian distribution, $\theta_{vib} \sim N(0,\sigma_{vib})$ and $\Delta\theta_{v,diff} \sim N(0,\sqrt{2\sigma_{vib}})$. Then, the average of A_{cov} is expressed by

$$E\,[A_{cov}] = \int_{-\infty}^{\infty} A_{cov}\,(\theta_{vib}, \Delta\theta_{v,diff})\, f_v\,(\theta_{vib})\, d\theta_{vib} \tag{22}$$

where the $f_v(\cdot)$ represents the PDF of θ_{vib}. Then, the total uncovered area is given by

$$A'_{unc}\,(\Delta\theta_{v,diff}) = A_{unc}\ (\Delta\theta_{v,diff}) - 2E\,[A_{cov}] \tag{23}$$

The hit probability of a single scan can be written as

$$P_{hit} = 1 - \int_{-\infty}^{\infty} \frac{A'_{unc}\,(\Delta\theta_{v,diff})}{A_{int}} f_{\Delta\theta_{v,\mathrm{diff}}}\,(\Delta\theta_{v,diff})\, d\Delta\theta_{v,diff} \tag{24}$$

where A_{int} is the area of region of interest and $f_{\Delta\theta\,v,diff}(\cdot)$ is the PDF of $\Delta\theta_{v,diff}$.

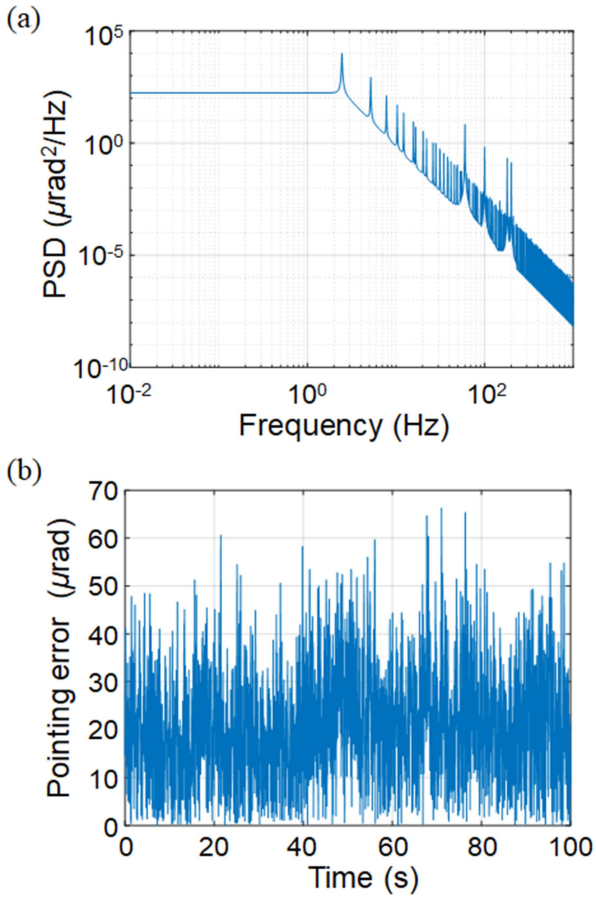

Fig. 4. (a) The power spectral density of an exemplary satellite vibration and (b) temporal radial pointing errors generated from the power spectral density.

When we fail to acquire the scan beam, the scans are repeated until the receiver satellite detects the scan beam successfully. In this multiple scan, when the receiver satellite acquires the scan beam at $(m+1)$th scan, the scan time and the overall hit probability are given by $T_{avg}+mT_{scan}$ and $(1-P_{hit})^m P_{hit}$, respectively. Thus, the average acquisition time for multiple scans under the satellite vibration is given by

$$T_{mult}=\sum_{m=0}^{\infty}(1-P_{hit})^m P_{hit}\,(T_{avg}+mT_{scan}) \tag{25}$$

III. Verification Through Simulation

In this section, we compare the theoretical analysis presented in the previous section with the Monte-Carlo simulation. For this purpose, we first emulate the satellite vibrations using the power spectral density (PSD) model, shown in Fig. 4(a) [8], [27], [28]. The vibrations are composed of harmonics of 2.5-Hz tones. They also include the frequency components at 65, 100, 175, and 200 Hz representing the mechanical vibrations caused by reaction wheels. By applying random phases to those spectral components, we generate angular fluctuations in the time domain as shown in Fig. 4(b). The standard deviation of this radial pointing error is 25 μrad. We next generate random orbital determination errors of the receiver satellite. These errors follow the Rayleigh distribution, as formulated in (12). The standard deviation is set to be 3.2 km on the receiver aperture plane [29]. The size of the uncertainty cone is set to be 3 sigma of the standard deviation of the receiver location error, which is calculated by dividing the transmission distance by the orbital determination error. For example, the half angle of uncertainty cone is set to be 9.6 mrad for the transmission distance of 1000 km. Under the angular fluctuations of the transmitter satellite, we carry out the acquisition procedure for the uncertainty cone using the spiral scan. Table I summarizes the system parameters used in this simulation. Finally, the average acquisition time is obtained through 5000 simulations.

TABLE I
Parameters of the Simulation

Symbol	Quantity	Value
k	overlap factor	0.2
T_{dw}	dwell time	2 ms
L	transmission distance	1000 km
P_t	transmit optical power	1 W
r_{rec}	receiver aperture radius	5 cm
E_{th}	energy threshold for detection	100 pJ
θ_{div}	divergence angle of scan beam	191.8 μrad
σ	standard deviation of error of receiver orbital determination	3.2 km
σ_{vib}	standard deviation of platform vibration of the transmitter satellite	25 μrad
N_{sim}	simulation number	5000

Fig. 5(a) shows the trajectory of the scan beam's footprints on the receiver's aperture plane in the absence of satellite vibrations. The footprints cover the entire region of the uncertainty area. However, in the presence of satellite vibrations, the trajectory is distorted and the beam footprints cannot cover the entire region of the uncertainty area. Fig. 5(b) shows a case when the standard deviation of the satellite's angular fluctuation is 100 μrad. The region uncovered by the footprint is painted in red.

Fig. 6 shows the hit probability of a single scan as a function of the effective angle of scan beam. It shows that our theoretical expression of (24) agrees with the simulation results. The discrepancy between the theoretical analysis and simulation tends to increase when the effective angle of scan beam is narrow and the angular fluctuation of satellite is large. This is because when the amount of vibration is much larger than the effective size of scan beam, the uncovered area [for example shown in Fig. 3(b)] could be covered by other rings. In our theoretical analysis, we consider only two rings, *not* bordering the region of

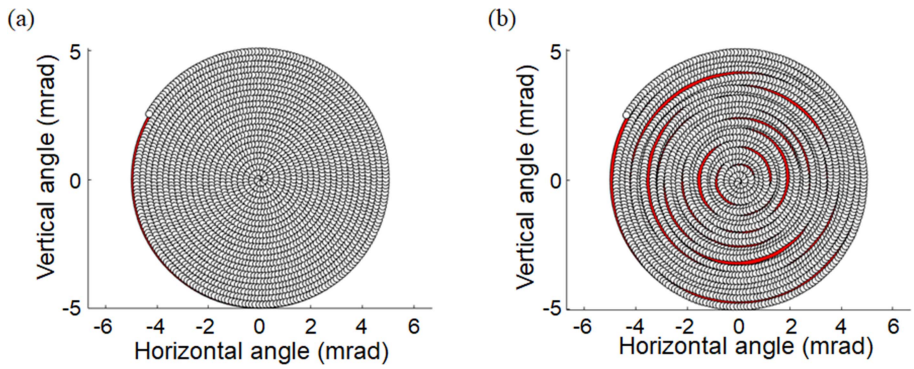

Fig. 5. Trajectory of scan beam's footprints on the receiver aperture plane (a) in the absence of vibrations and (b) in the presence of vibrations. The standard deviation of vibration is 100 μrad. The region uncovered by the footprint is painted in red.

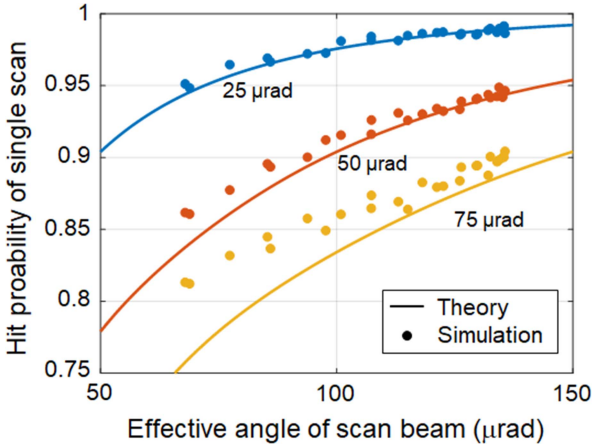

Fig. 6. Hit probability to the effective angle of scan beam for a couple of standard deviations of angular fluctuation.

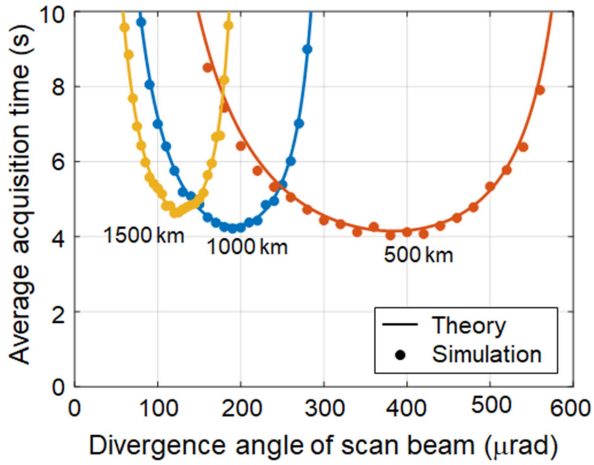

Fig. 7. Average acquisition time versus the divergence angle of the scan beam for a couple of transmission distances.

interest. Thus, our theoretical analysis presents the conservative estimation of the hit probability.

Fig. 7 shows the average acquisition time simulated for a couple of transmission distances when the standard deviation

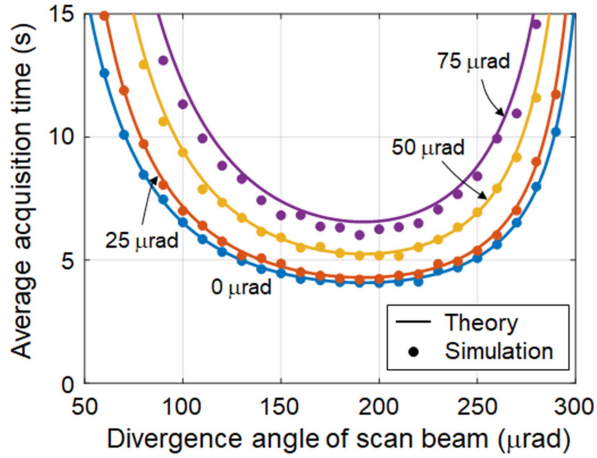

Fig. 8. Average acquisition time as a function of divergence angle of scan beam for a few standard deviations of angular fluctuation.

of angular fluctuation is 25 μrad. Also plotted in this figure for comparison are the theoretical results of (25). Our theoretical analysis agrees well with the simulation results. The figure shows that the optimum divergences for acquisition time are 384, 192, and 128 μrad for the transmission distances of 500, 1000, and 1500 km, respectively. As the transmission distance increases, the effective angle of scan beam should be decreased, as formulated by (15). This might imply that the acquisition time should also be increased with the transmission distance. However, the orbital determination error is fixed, regardless of transmission distance, which in turn, implies that the size of uncertainty cone (expressed in radian) is decreased as the transmission distance increases. Consequently, the minimum average acquisition time increases slightly with the transmission distance.

The average acquisition time under various standard deviations of satellite vibrations is shown in Fig. 8. The transmission distance is 1000 km. It shows that the optimum beam divergence angle for acquisition time is independent of the amount of vibration. It is estimated to be 192 μrad, as expressed in (16). However, the mechanical vibrations of satellites reduce the hit probability of a single scan, and thus the number of multiple

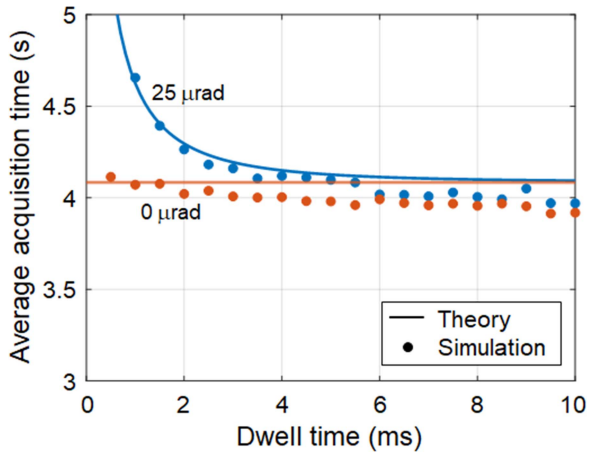

Fig. 9. Average acquisition time versus the dwell time. The numbers next to the graphs are the standard deviations of angular fluctuation.

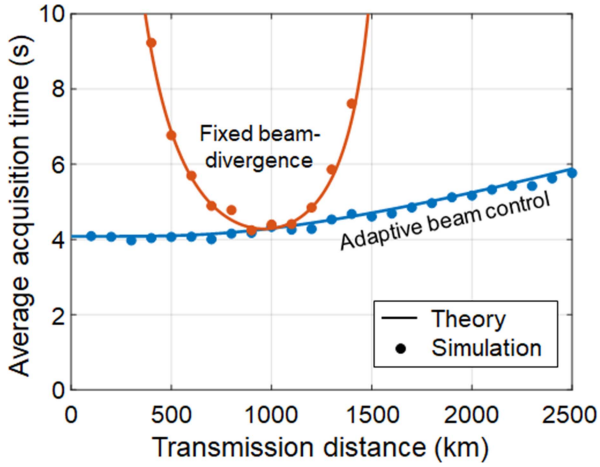

Fig. 10. Comparison of the acquisition time between the adaptive beam control and fixed beam-divergence schemes.

scans increases with the amount of vibrations. For example, the average acquisition time is increased from 4.1 to 6.6 seconds when the standard deviation of vibration rises from 25 to 75 μrad.

We next investigate the impact of the dwell time on the average acquisition time. Fig. 9 shows the average acquisition time versus the dwell time. The divergence angle of scan beam for each dwell time is set to be the optimum value for the acquisition time. The results show that the acquisition time is independent of the dwell time in the absence of vibration. This is because even though the scan time increases with T_{dw}, as shown in (14), the effective angle of scan beam also decreases with T_{dw}. In the presence of vibrations, on the other hand, the average acquisition time increases as the dwell time decreases due to the multiple scans resulting from the reduced size of effective angle of scan beam. Our theoretical results agree well with the simulation results.

We compare the acquisition time of the ABC scheme with that of the fixed beam-divergence scheme. Fig. 10 shows the results.

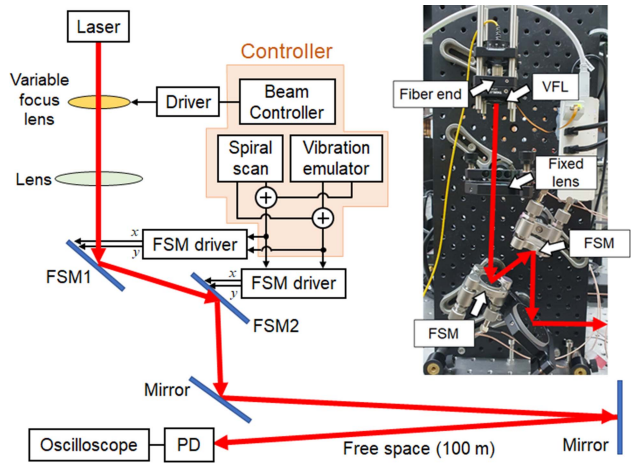

Fig. 11. Experimental setup. The inset shows the photo of the transmitter apparatus.

The standard deviation of angular fluctuation is 25 μrad. For the fixed beam-divergence scheme, we set the beam divergence to be 192 μrad. The ABC scheme adjusts the beam divergence angle adaptively to the transmission distance, according to our theoretical analysis of (16). The results clearly show that the ABC scheme outperforms the fixed beam-divergence scheme over a wide range of transmission distances. For example, the acquisition time of the ABC scheme is 3 times shorter than that of the fixed beam-divergence scheme when the transmission distance is 1500 km.

IV. Verification Through Experiment

We also carry out a proof-of-concept experiment to validate our theoretical analysis. The experimental setup is shown in Fig. 11. The optical beam generated from a fiber-pigtailed laser diode propagates through a double-lens configuration, which consists of a VFL and a fixed-focus lens. Here, the wavelength of the laser is 1550 nm and the optical power of the beam is set to be 10 dBm. The VFL (Optotune EL-10-30-TC-NIR-12D) used in the experiment comprises a container filled with optical liquid and an elastic polymer membrane sealing. The lens has an electromagnetic actuator that exerts pressure on the container, which, in turn, changes the curvature of the lens proportional to the pressure on the container. Electric current then controls the focal length of the lens through the coil of the actuator. The VFL has a clear aperture of 10 mm and has a range of focal length from 5 to 12 cm. The fixed-focus lens has a focal length of 100 mm and a diameter of 50.8 mm. The double-lens configuration allows us to generate a narrow optical beam for laser ISL applications limited by the small size of VFL [25]. By using this configuration, we can vary the divergence angle of the transmitter beam from 98 to 230 μrad in this experiment. The optical beam is reflected by a couple of fast steering mirrors (FSMs). The FSM having a diameter of 25.4 mm utilizes piezo-electric adjusters and has a maximum steering range of 1 mrad in x and y directions. We utilize two FSMs to increase the steering range of the transmitting beam. The FSMs are controlled by

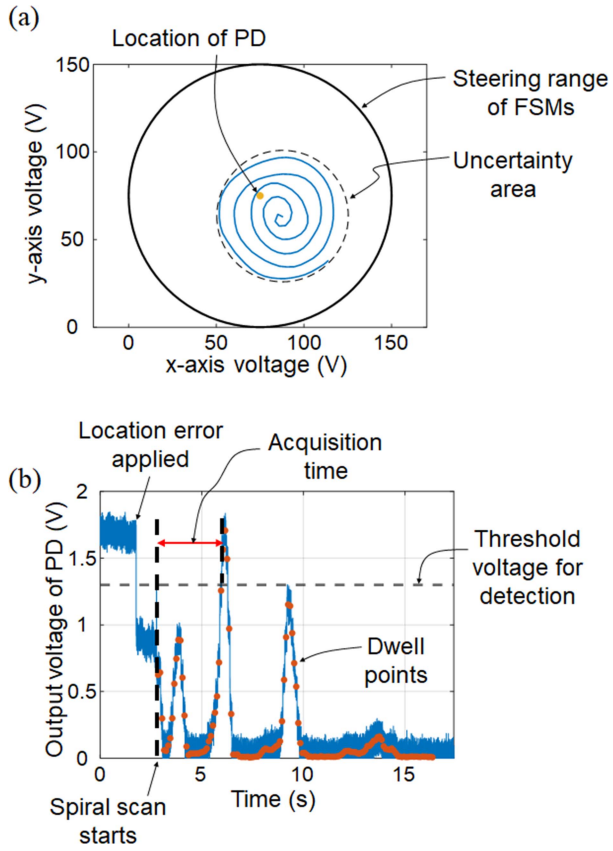

Fig. 12. (a) Exemplary spiral trajectory as functions of voltages applied to FSMs. (b) Exemplary output voltage detected by the PD over time.

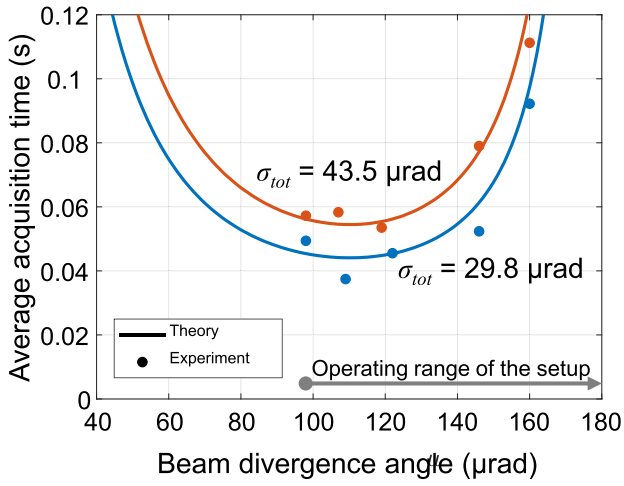

Fig. 13. Measured average acquisition time versus the beam divergence angle.

using a personal computer to realize the spiral scan. In order to emulate the satellite vibrations, we add the pointing errors deliberately as shown in Fig. 4(b) to the FSM driving signals. The inset of Fig. 11 shows the photo of the transmitter setup. To minimize the distortions of beam quality induced by gravity, we arrange the optical axis of VFL vertically and then deflect the optical beam horizontally by using a mirror [26]. The optical beam propagates along the corridor of a building to a flat mirror (having a clear aperture of 100 mm) placed 50 m away from the transmitter and then comes back to the detector. Thus, the transmission distance is 100 m. The optical beam is received by using a photo-detector (PD) having an active area of 3.14 mm^2.

Unlike the inter-satellite laser links where the accurate location of the counter satellite is unknown before the acquisition procedure, the location of the PD can be readily identified in lab experiment. Thus, we generate the location error deliberately before the beginning of acquisition procedure in our experiment. The location errors are set to follow the 2-dimensional Gaussian distribution having zero means and standard deviations of 0.33 mrad. The size of uncertainty cone is set to be 1 mrad. Fig. 12(a) shows the exemplary spiral scan displayed in terms of the x- and y-direction voltages applied to FSMs. The PD is located at the center of the steering range of FSMs. Since we apply a location error deliberately, the starting point of the spiral scan is positioned away from the PD's location. The spiral scan is performed until it covers the uncertainty area. Due to the satellite vibrations (standard deviation of 14.4 μrad) emulated in the experiment, we can see that the spiral trajectory is distorted.

Fig. 12(b) shows the output voltage of the PD over time. The curve in this plot exhibits the photo-voltage detected by the PD. Due to the scintillation in our experiment, the received optical power fluctuates over time even though the setup is stationary. Thus, we increase the measurement time to 100 ms and average out the scintillation-induced power fluctuations in each dwell point. The averaged optical power is used to calculate the energy collected by the PD over the dwell time. The dwell time is set to be 2 ms in the experiment. We believe that this power averaging would not be required in inter-satellite links due to the absence of atmospheric turbulence. In the figure, we see that the location error is applied 1.8 second after the measurement starts. The spiral scan starts at about 2.8 second in the figure. We observe three peaks in this curve. As the spiral scan beam approaches the location of the PD, the output voltage of PD increases. We acquire the location of the PD when the photo-voltage exceeds the threshold voltage for detection, which is set to be 1.3 V in our experiment.

Fig. 13 shows the measured average acquisition time as a function of the beam divergence angle. Also plotted in this figure for comparison are the theoretical results. The operating beam divergence angle of our double-lens configuration ranges from 98 to 230 μrad. We generate 50 cases of location errors to obtain the average acquisition time. It should be noted that the time required to average out the power fluctuations (i.e., 100 ms for each dwell point) is not included in the acquisition time. Due to the open-loop control of FSMs, they experience a hysteresis, which serve as additional pointing errors in our experiment. The average error arising from the hysteresis is estimated to be 25.9 μrad. For the emulation of vibration, we generate pointing errors having standard deviations of 14.7 and 35 μrad. Thus, the total pointing errors induced by hysteresis and emulation should be 29.8 [$=(25.9^2 + 14.7^2)^{1/2}$] and 43.5 [$=(25.9^2 + 35^2)^{1/2}$] μrad. The results show that the measured acquisition time agrees very well with the theoretical values. The minimum acquisition times are measured to be 37.4 and 53.5 ms for 29.8- and 43.5-μrad

standard deviations of pointing error, respectively. They are all achieved for the beam divergence angle of $\sim$110 μrad.

V. Conclusion

We have analyzed the acquisition time of laser inter-satellite links in the presence of satellite vibrations. The mechanical vibrations caused by, for example, thrust firing and mechanical moving components, give rise to pointing errors and serve to distort the spiral trajectory of scan beam for acquisition. We derive the analytic expression about the average acquisition time and the optimum beam divergence angle for minimizing the acquisition time. Our theoretical analyses are validated by Monte-Carlo simulations and the proof-of-concept experiment. The results confirm that our theory estimates the acquisition time accurately over a wide range of transmission distances in the presence of satellite vibrations. Also, we show that the acquisition time could be minimized by adjusting the beam divergence angle adaptively to the link conditions. The findings of this work could be used for the design of spiral trajectory of the scan beam and for the control of beam divergence angle under the PAT procedure.

Acknowledgment

The authors would like to thank Prof. Hyosang Yoon for useful discussions on the uncertainty area and orbital determination errors.

References

[1] M. Toyoshima, "Trends in satellite communications and the role of optical free-space communications," *J. Opt. Netw.*, vol. 4, no. 6, pp. 300–311, May 2005.

[2] H. Kaushal and G. Kaddoum, "Optical communication in space: Challenges and mitigation techniques," *IEEE Commun. Surveys Tut.*, vol. 19, no. 1, pp. 57–96, Firstquarter 2017.

[3] M. A. Khalighi and M. Uysal, "Survey on free space optical communication: A communication theory perspective," *IEEE Commun. Surveys Tut.*, vol. 16, no. 4, pp. 2231–2258, Fourthquarter 2014.

[4] C. Carrizo, M. Knapek, J. Horwath, D. Gonzalez, and P. Cornwell, "Optical inter-satellite link terminals for next generation satellite constellations," in *Proc. Soc. Photographic Instrum. Eng. Free-Space Laser Commun. 32nd*, 2020, vol. 11272, pp. 8–18.

[5] T. Nielsen, "Pointing acquisition and tracking system for the free space laser communication system, SILEX," *Proc. SPIE*, vol. 2381, pp. 194–205, 1995.

[6] *Optical High Data Rate (HDR) Communication–1064 nm*, Standard CCSDS 141.11-O-1, Dec. 2018.

[7] B. Rodiger, R. Ruddenklau, C. Schmidt, and M. Lehmann, "Acquisition concept for optical inter-satellite communication terminals on CubeSats," in *Proc. Small Satell. Syst. Serv. 4S Symp.*, 2022.

[8] M. Toyoshima, Y. Takayama, H. Kunimori, T. Jono, and S. Yamakawa, "In-orbit measurements of spacecraft microvibrations for satellite laser communication links," *Opt. Eng.*, vol. 49, no. 8, Aug. 2010, Art. no. 083604.

[9] K. Baeck, "Analytic evaluation of pointing error on free-space optical communication satellite," M.S. thesis, Dept. Aerosp. Eng., South Korea Adv. Inst. Sci. Technol., Daejeon, South Korea, 2021.

[10] J. Wang, J. Kahn, and K. Lau, "Minimization of acquisition time in short-range free-space optical communication," *Appl. Opt.*, vol. 41, no. 36, pp. 7592–7602, Dec. 2002.

[11] E. Clements et al., "Nanosatellite optical downlink experiment: Design, simulation, and prototyping," *Opt. Eng.*, vol. 55, no. 11, pp. 111610–111610, Sep. 2016.

[12] Z. Sodnik, H. Lutz, B. Furch, and R. Meyer, "Optical satellite communications in Europe," *Proc. SPIE*, vol. 7587, pp. 49–57, 2010.

[13] S. Gagnon et al., "Recent developments in satellite laser communications: Canadian context," in *Proc. Int. Conf. Space Opt. Syst. Appl.*, 2012, pp. 9–12.

[14] H. Kaushal, V. Jain, and S. Kar, *Free Space Optical Communication*. Berlin, Germany: Springer, 2017.

[15] U. Sterr, M. Gregory, and F. Heine, "Beaconless acquisition for ISL and GL, summary of 3 years operation in space and on ground," in *Proc. Int. Conf. Space Opt. Syst. Appl.*, 2011, pp. 38–43.

[16] C. Hindman and L. Robertson, "Beaconless satellite laser acquisition-modeling and feasibility," in *Proc. IEEE Mil. Commun. Conf.*, 2004, vol. 1, pp. 41–47.

[17] M. Zhang, B. Li, and S. Tong, "A new composite spiral scanning approach for beaconless spatial acquisition and experimental investigation of robust tracking control for laser communication system with fluctuation," *IEEE Photon. J.*, vol. 12, no. 6, Dec. 2020, Art. no. 7906212.

[18] X. Li, S. Yu, J. Ma, and L. Tan, "Analytical expression and optimization of spatial acquisition for intersatellite optical communications," *Opt. Exp.*, vol. 19, no. 3, pp. 2281–2390, Jan. 2011.

[19] J. Wang, B. Li, T. Zhao, and Y. Sun, "Space optical communication system with a sub-second acquisition time," *Opt. Lett.*, vol. 47, no. 23, pp. 6085–6088, Dec. 2022.

[20] L. Friederichs, U. Sterr, and D. Dallmann, "Vibration influence on hit probability during beaconless acquisition," *J. Lightw. Technol.*, vol. 34, no. 10, pp. 2500–2509, May 2016.

[21] A. Yariv and P. Yeh, "Rays and optical beams," in *Photonics: Optical Electronics in Modern Communications*, 6th ed. London, U.K.: Oxford Univ. Press, 2006.

[22] A. Farid and S. Hranilovic, "Outage capacity optimization for free-space optical links with pointing errors," *J. Lightw., Tehcnol.*, vol. 25, no. 7, pp. 1702–1710, Jul. 2007.

[23] V. Mai and H. Kim, "Beaconless PAT and adaptive beam control using variable focus lens for free-space optical communication system," *Appl. Phys. Lett. Photon.*, vol. 6, 2021, Art. no. 020801.

[24] V. Mai and H. Kim, "Adaptive beam control techniques for airborne free-space optical communication systems," *Appl. Opt.*, vol. 57, no. 26, pp. 7462–7471, Sep. 2018.

[25] K. Lee, V. Mai, and H. Kim, "Dynamic adaptive beam control system using variable focus lenses for laser inter-satellite link," *IEEE Photon. J.*, vol. 14, no. 4, Aug. 2022, Art. no. 7337108.

[26] V. V. Mai and H. Kim, "Non-mechanical beam steering and adaptive beam control using variable focus lenses for free-space optical communications," *J. Lightw. Technol.*, vol. 39, no. 24, pp. 7600–7608, Dec. 2021.

[27] Y. Teng, M. Zhang, and S. Tong, "The optimization design of sub-regions scanning and vibration analysis for beaconless spatial acquisition in the inter-satellite laser communication system," *IEEE Photon. J.*, vol. 10, no. 6, Dec. 2018, Art. no. 7909611.

[28] D. Yu, G. Wany, and Y. Zhao, "On-orbit measurement and analysis of the micro-vibration in a remote-sensing satellite," *Adv. Astronaut. Sci. Technol.*, vol. 1, no. 2, pp. 191–195, Dec. 2018.

[29] K. Riesing, "Orbit determination from two line element sets of ISS-deployed CubeSats," in *Proc. 29th Annu. Amer. Inst. Aeronaut. Astronaut./Utah State Univ. Conf. Small Satell.*, Logan, UT, USA, 2015, Paper SSC15-VIII-5.